Title	Insight into the impact of atomic- and nano-scale indium distributions on the optical properties of InGaN/GaN quantum well structures grown on m-plane freestanding GaN substrates
Authors	Tang, Fengzai;Zhu, Tongtong;Fu, Wai-Yuan;Oehler, Fabrice;Zhang, Siyuan;Griffiths, James T.;Humphreys, Colin;Martin, Tomas L.;Bagot, Paul A. J.;Moody, Michael P.;Patra, Saroj K.;Schulz, Stefan;Dawson, Philip;Church, Stephen;Jacobs, Janet;Oliver, Rachel A.
Publication date	2019-06-11
Original Citation	Tang, F., Zhu, T., Fu, W.-Y., Oehler, F., Zhang, S., Griffiths, J. T., Humphreys, C., Martin, T. L., Bagot, P. A. J., Moody, M. P., Patra, S. K., Schulz, S., Dawson, P., Church, S., Jacobs, J. and Oliver, R. A. (2019) 'Insight into the impact of atomic- and nano-scale indium distributions on the optical properties of InGaN/GaN quantum well structures grown on m-plane freestanding GaN substrates', Journal of Applied Physics, 125(22), 225704, (13 pp). doi: 10.1063/1.5097411
Type of publication	Article (peer-reviewed)
Link to publisher's version	https://aip.scitation.org/doi/abs/10.1063/1.5097411 - 10.1063/1.5097411
Rights	© 2019 Author(s). Published under license by AIP Publishing.
Download date	2025-01-07 02:33:22
Item downloaded from	https://hdl.handle.net/10468/8415

Fengzai Tang, Tongtong Zhu, Wai-Yuan Fu, Fabrice Oehler, Siyuan Zhang, James T. Griffiths, Colin Humphreys, Tomas L. Martin, Paul A. J. Bagot, Michael P. Moody, Saroj Kanta Patra, Stefan Schulz, Philip Dawson, Stephen Church, Janet Jacobs, and Rachel A. Oliver

View Online   Export Citation   CrossMark

ARTICLES YOU MAY BE INTERESTED IN

Journal of Applied Physics   Special Topic: Molecular Spintronics

AIP Publishing

Insight into the impact of atomic- and nano-scale indium distributions on the optical properties of InGaN/GaN quantum well structures grown on *m*-plane freestanding GaN substrates

Fengzai Tang,[1,a] Tongtong Zhu,[1] Wai-Yuan Fu,[1] Fabrice Oehler,[1,b] Siyuan Zhang,[1] James T. Griffiths,[1] Colin Humphreys,[1] Tomas L. Martin,[2] Paul A. J. Bagot,[2] Michael P. Moody,[2] Saroj Kanta Patra,[3,4] Stefan Schulz,[4] Philip Dawson,[5] Stephen Church,[5] Janet Jacobs,[5] and Rachel A. Oliver[1,c]

AFFILIATIONS

[1] Department of Materials Science and Metallurgy, University of Cambridge, 27 Charles Babbage Road, Cambridge CB3 0FS, United Kingdom
[2] Department of Materials, University of Oxford, Parks Road, Oxford OX1 3PH, United Kingdom
[3] Department of Electrical Engineering, University College Cork, Cork T12YN60, Ireland
[4] Photonics Theory Group, Tyndall National Institute, Dyke Parade, Cork T12R5CP, Ireland
[5] Photon Science Institute, School of Physics and Astronomy, University of Manchester, Manchester M13 9PL, United Kingdom

[a]**Present address:** Warwick Manufacturing Group, University of Warwick, Lord Bhattacharyya Way, Coventry CV4 7AL, United Kingdom.
[b]**Present address:** Centre for Nanoscience and Nanotechnology, CNRS, Université Paris-Sud, Université Paris-Saclay, Route de Nozay, 91460 Marcoussis, France.
[c]**Electronic mail:** rao28@cam.ac.uk.

ABSTRACT

We investigate the atomic scale structure of *m*-plane InGaN quantum wells grown on bulk *m*-plane GaN templates and reveal that as the indium content increases there is an increased tendency for nonrandom clustering of indium atoms to occur. Based on the atom probe tomography data used to reveal this clustering, we develop a $\mathbf{k} \cdot \mathbf{p}$ model that takes these features into account and links the observed nanostructure to the optical properties of the quantum wells. The calculations show that electrons and holes tend to colocalize at indium clusters. The transition energies between the electron and hole states are strongly affected by the shape and size of the clusters. Hence, clustering contributes to the very large line widths observed in the experimental low temperature photoluminescence spectra. Also, the emission from *m*-plane InGaN quantum wells is strongly linearly polarized. Clustering does not alter the theoretically predicted polarization properties, even when the shape of the cluster is strongly asymmetric. Overall, however, we show that the presence of clustering does impact the optical properties, illustrating the importance of careful characterization of the nanoscale structure of *m*-plane InGaN quantum wells and that atom probe tomography is a useful and important tool to address this problem.

Published under license by AIP Publishing. https://doi.org/10.1063/1.5097411

I. INTRODUCTION

Commercial blue light emitting diodes (LEDs) are generally grown on the *c*-plane (0001) of wurtzite GaN substrates or pseudo-substrates and have an active region composed of InGaN/GaN quantum wells (QWs). In these devices, an external quantum efficiency as high as 70%–80% can be achieved at room temperature,[1,2] despite the presence of threading dislocations with densities of $10^8 \, \text{cm}^{-2}$ or above,[3] which act as nonradiative recombination

centers and might be expected to degrade device performance.[4] Carrier localization is believed to prevent carrier diffusion to dislocation cores and thus accounts for the high room temperature internal quantum efficiency of light emission from InGaN QWs.[5] Evidence for such localization is seen in experimental observation of an "S-shaped" temperature dependence of the peak photoluminescence (PL) energy, the PL line width, and the occurrence of a "mobility edge."[6–8]

Indium atom clustering in c-plane InGaN QWs was initially considered to be the main origin of carrier localization in these systems.[9] However, pioneering atom probe tomography (APT) analysis by Galtrey et al.[10] found that indium clustering is not a prerequisite for efficient emission from InGaN QWs. The absence of statistically significant nonrandom indium clustering was later confirmed by careful transmission electron microscopy (TEM) investigations.[11]

Despite the commercialization of LEDs, devices grown on the c-plane orientation suffer from spontaneous electric polarization, because of the noncentrosymmetric wurtzite crystal structure.[12] Since InGaN has larger lattice parameters than GaN, epitaxial InGaN layers grown on GaN experience a compressive strain in the growth plane (c-plane), leading to a strain dependent piezoelectric polarization field in the c-direction. The magnitude of the total electrostatic built-in field depends on the metallic site fraction, x, in $In_xGa_{1-x}N$, and field values of the order of 10^6 V/cm along the polar c-direction (perpendicular to the QW layers) have been reported.[12,13,14,15] This leads to spatial separation of the electron and hole wave functions in the well along the growth direction, the so-called quantum-confined Stark effect (QCSE), reducing the probability of radiative recombination. In the presence of competing nonradiative recombination pathways, this can be a contributory factor to the degradation of the internal quantum efficiency of the emission.[16,17] This issue is particularly pressing in green and amber emitting LEDs, which exhibit much lower efficiencies than their blue counterparts and is referred to as the "green gap" problem.[1,2,18,19] While the precise cause of the green gap is controversial, the decreased electron–hole wavefunction overlap in QWs at higher indium contents is frequently cited as a contributory factor.[2]

InGaN QWs grown on nonpolar crystal orientations [such as m-plane (1–100) and a-plane (11–20)] are ideally free of macroscopic built-in electrostatic fields; this provides a potential route to fabricate green emitting devices with improved optical performance because of the increased electron–hole wavefunction overlap. This is the motivation behind our efforts to study the structural and optical properties of nonpolar QWs with varying indium contents and to specifically investigate the role of the indium distribution in controlling the optical properties of QW systems emitting at longer wavelengths. This allows us to assess the suitability of such materials to help overcome the green gap or to contribute to other optoelectronic applications.

In general, the optical properties of nonpolar QWs exhibit a number of distinctive features, including significantly shorter radiative lifetimes than are observed in the polar c-plane case due to the absence of macroscopic built-in electric fields.[20] Furthermore, nonpolar m-plane QW structures also show emission of highly linearly polarized light. Fundamentally, this originates from valence band splitting effects induced by the asymmetric in-plane biaxial stress on nonpolar InGaN QWs and differences in the effective

masses of the different valence bands along the growth direction.[21] While a-plane QWs also exhibit polarized emission, the degree of optical linear polarization (DOLP) is typically lower and also varies across the spectrum.[20] In 2016, Tang et al. reported the observation of indium clusters constituting a significant deviation from a random distribution in a-plane InGaN QWs using APT, in contrast to the statistically random indium distribution observed in c-plane QWs of approximately the same composition.[22] We have tentatively suggested that the presence of clustering in the a-plane may be linked to the low and wavelength dependent DOLP observed in this system.[20]

In this work, utilizing both aberration-corrected TEM[2,23] and APT[24,25] techniques, we have studied InGaN/GaN QWs grown on m-plane ammonothermal bulk GaN substrates down to the atomic level. The use of bulk GaN substrates minimizes the influence of crystalline defects on the optical properties.[26] The variations in the observed structure with indium content are correlated with measurements of the optical properties of the same structure,[20] and their interrelation was assessed using a theoretical framework consisting of a continuum-based model that accounts for InGaN clusters inside nonpolar InGaN/GaN QWs. The theoretical model takes input from both the APT data and results from atomistic calculations for the material input parameters. The combination of the microstructural and theoretical studies, in conjunction with our earlier studies of the optical properties of these materials, allows us to address the impact of microstructure on optical properties in m-plane InGaN QWs, including the question of how clustering affects the DOLP in nonpolar systems.

II. EXPERIMENTAL METHODS AND THEORETICAL BACKGROUND

A. Experiment

Three m-plane samples containing 5-period InGaN/GaN QW structures were grown on ammothermal bulk GaN substrates using metal organic vapor phase epitaxy (MOVPE) in a Thomas Swan $6 \times 2''$ close-coupled showerhead reactor. The GaN substrates used had a miscut of $2.0 \pm 0.2°$ toward the ($-c$)-direction and a nominal threading dislocation density less than 5×10^4 cm^{-2}. Trimethyl-gallium, trimethyl-indium, and ammonia were used as precursors, and hydrogen and nitrogen as carrier gases for the GaN buffer and InGaN QW growth, respectively. A $2\,\mu m$ undoped GaN buffer layer was grown on the substrates at 1050 °C at a pressure of 100 Torr, prior to the growth of the 5-period InGaN/GaN QW structure. The InGaN QWs in the three samples were grown at temperatures of 745 °C, 735 °C, and 705 °C, respectively. All samples utilized the same III/V ratio of 23 000 for QW growth and a pressure of 300 Torr. After the growth of each InGaN layer, a 1 nm GaN barrier was grown at the same InGaN growth temperature. The GaN barrier continued to grow as the temperature was ramped to 855 °C in 90 s at which point the GaN barrier was completed, giving a total barrier thickness of ∼6 nm. This growth method is known as quasi-two-temperature growth.[27]

XRD analysis was carried out on a Philips/Panalytical PW3050/65 X'Pert PRO high resolution horizontal diffractometer. As will be explained in more detail later, the indium content of the QWs increased with decreasing QW growth temperature.

The samples grown at 745 °C, 735 °C, and 705 °C will thus hereafter be designated "Low," "Med," and "High," indicating the lowest, medium, and highest indium contents, respectively. Cross-sectional TEM samples and APT samples were prepared using a dual-beam focused ion beam microscope (FIB: FEI Helios NanoLab™) through an *in situ* lift-out approach, in which a final clean-up procedure involving combined low FIB voltages and currents was used to minimize beam-induced damage to the samples.[28] The TEM lamellae were prepared with an approximately *a*-direction[11–20] surface normal, and the APT samples were mounted on a standard silicon (Si) coupon with an array of preshaped flat-topped Si posts. A TEM microscope (FEI Titan[3] 80–300 kV) with a probe corrector was used for high resolution STEM (scanning TEM) imaging at 300 kV, where the image was acquired while the electron beam was parallel to the *a*-zone axis[11–20] of the sample. HAADF (high-angle annular dark field) images in STEM mode were acquired with inner cut-off semicollection angles between about 23 and 60 mrads.

APT analysis was conducted on a CAMECA LEAP 3000× HR instrument, which was fitted with a high resolution reflectron mass spectrometer and a laser emitting at 532 nm. The analysis was conducted in pulsed laser mode with a nominal pulse duration of 12 ps and a 10 μm spot size. The three samples with Low, Med, and High indium contents were analyzed at about 0.004–0.02 nJ per pulse, and a detection rate of on average 0.005–0.01 ions per pulse. In these experiments, a constant pulse repetition rate of 200 kHz was used, and the temperature of the sample stage was maintained at around 30 K. APT 3D (three-dimensional) reconstruction was performed using the CAMECA IVAS™ and calibrated with the assistance of information as to the thickness of QW and/or the geometry of APT sample obtained from electron microscopy images and correlated with the X-ray diffraction data. In order to minimize the effect of through-thickness compositional variations in the QW, we used a similar statistical analysis approach as detailed in Ref. 22, namely, a statistical frequency distribution (FD) analysis of indium distribution carried out on the extracted subvolume of each QW. In this analysis, the measured frequency distribution of the indium content is compared to the expected distribution for a random alloy and the values of χ^2, and the significance level or p-value are calculated. In order to reject the null hypothesis that the alloy is random, it is usual to require a value of $p < 0.05$ (5%). The subvolume of QW was isolated using half the maximum indium fraction measured perpendicularly through the face of the QW. In addition to this FD analysis, a modified nearest neighbor (NN) approach that was developed in studying *a*-plane QWs[22] was employed, involving artificially projecting all indium and Ga (gallium) atoms into a single plane before assessing the nearest neighbor distances and comparing to those in a randomized data set.

To gain insight into the optical properties of the QW systems, polarization dependent photoluminescence (PL) measurements were conducted using excitation from a continuous wave (CW) He/Cd laser. The *c*-axis of the GaN was held horizontally in order to evaluate the spectral dependence of the DOLP, $\rho(T)$, given by

$$\rho(T) = \frac{I_\perp(T) - I_\parallel(T)}{I_\perp(T) + I_\parallel(T)}. \qquad (1)$$

Here, T is the sample temperature and $I_\perp$ and $I_\parallel$ are the PL intensities polarized perpendicular and parallel to the *c*-axis of the sample, respectively. The samples were mounted on the cold finger of a closed cycle cryostat, which enabled the sample temperature to be controlled between 10 K and room temperature ($T = 300$ K). The experimental details are reported elsewhere.[20]

B. Theoretical framework

The main target of the theoretical modeling is to gain insight into the impact of indium clustering effects on the electronic and optical properties of nonpolar InGaN/GaN QWs. As with the experimental studies, special attention is paid to the influence of the indium content on the results. To address these questions, $\mathbf{k} \cdot \mathbf{p}$ studies have been performed in which the QW is treated as a three-dimensional (3D) object instead of the "standard" one-dimensional approximation. The 3D description is required to address indium clustering effects in the well, which will be presented below. Here, we briefly summarize the main ingredients of the underlying $\mathbf{k} \cdot \mathbf{p}$ model. More information on the theoretical framework can be found in Refs. 29 and 30. For the hole states, the model builds on a six-band Hamiltonian, thus accounting for band mixing effects. For the electrons a single-band approach has been applied. We also account for strain effects as well as spontaneous and piezoelectric polarization fields. Overall, a symmetry adapted theoretical framework has been used.[31] The relevant material parameters are given in Ref. 32. It should be noted that composition dependent bandgap, conduction, and valence band edge bowing parameters have been employed. These quantities have been extracted from atomistic tight-binding calculations,[33] which account for random alloy fluctuations and thus connected carrier localization effects.

III. RESULTS AND DISCUSSION

A. Experiment

1. Structural analysis of QWs

The nanostructures of the QWs in the three samples were examined by cross-sectional TEM analysis as illustrated in Fig. 1. The electron beam was parallel to the *a*-direction. Figures 1(a) and 1(b) are from the Low indium content sample, and Figs. 1(c) and 1(d) are from the samples with Med and High indium contents, respectively. At a relatively low magnification, the InGaN QWs appear fairly uniform in all samples, as illustrated in Fig. 1(a) for the case with Low indium content. At higher magnifications, the QWs in the samples with Low and Med indium contents [Figs. 1(b) and 1(c)] still appear uniform, whereas some uneven contrast in the QWs of the High indium content sample is visible, as shown in Fig. 1(d), where some of the inhomogeneities are labelled by arrows. An increased thickness of InGaN QW layers can also be seen with increasing indium contents, that is, the QW width increases from 2.1 ± 0.2 nm to 2.3 ± 0.2 and 2.6 ± 0.3 nm across the three samples, as summarized in Table I. However, the thicknesses of the barriers are relatively constant across all three samples being in the range of 5.7–5.8($\pm$0.4) nm. This is in agreement with the XRD measurement of the three samples, where the thickness of QWs was measured to be in the range of
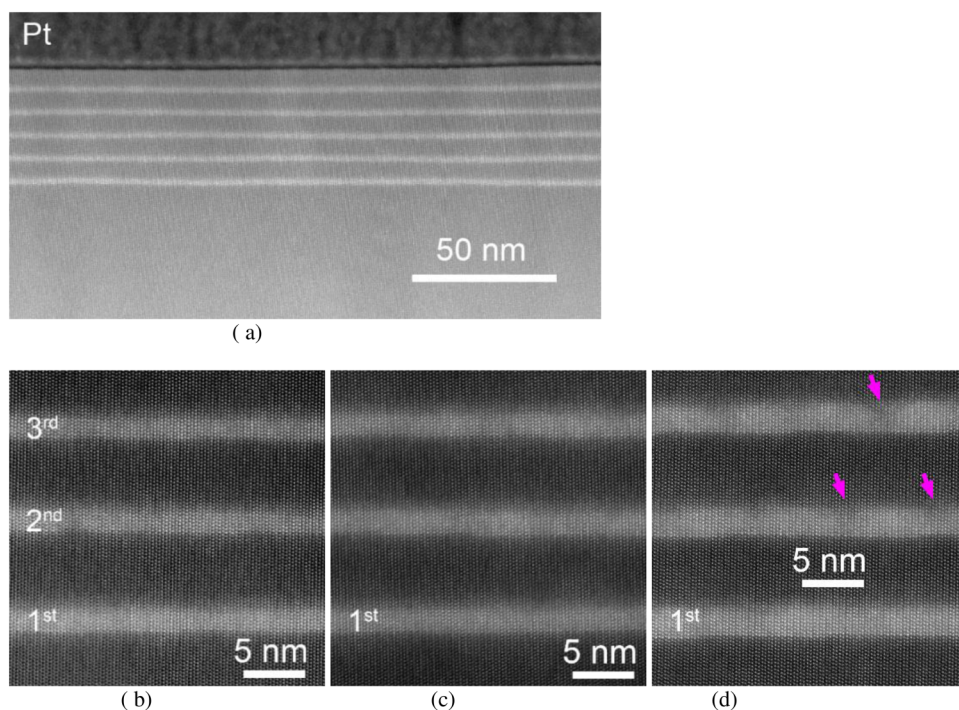
FIG. 1. STEM-HAADF images of the multiple QW samples. (a) A wide view of 5QWs from the Low indium content sample, and (b)–(d) showing the first 3QWs closest to the GaN substrates from the samples with Low, Med, and High indium contents, respectively. In (d), the pink arrows indicate inhomogeneities in the QW.

1.9–2.4(±0.2) nm and that of the GaN barrier was relatively constant, about 6.1 ± 0.3 nm.

Since the HAADF image is essentially formed by the incoherent Rutherford-scattered electrons, revealing the elemental atomic number (z) contrast,[34] the intensity of an atomic column in an image relates to the amount of indium in the InGaN QW layers. The apparent "blotchy" areas (contrasts) in the QWs in the High indium content sample thus suggest an inhomogeneous indium distribution. It should be noted that high energy beam damage, including both TEM beam and FIB ion beam, may lead to the apparent indium clustering in the high resolution TEM analysis.[35,36]

A 3D APT reconstruction of the High indium content QW structure is depicted in Fig. 2(a) (box size $45 \times 45 \times 55$ nm^3), in which only the reconstructed indium atoms are shown (for visual clarity). From Fig. 2(a), the second QW (defining the second QW as the second one to be grown, or the second closest to the original GaN substrate) was extracted (box size $45 \times 45 \times 11$ nm^3). The indium distribution within this QW may be visually assessed in Fig. 2(b), which shows a tilted view of the QW (the GaN barriers on either side are not shown). Note that, following a previously

established notation, the upper GaN barrier, as well as the upper interfaces, of each QW refers to the barrier or interface which is furthest away from the original substrate.[22] Although Fig. 2(b) is suggestive of some degree of inhomogeneity in the indium atom distribution, it is essential to carry out statistical analysis to verify this suggestion.

One-dimensional indium content profiles across the 5 QWs for all three samples are shown in Fig. 2(c). The indium content in each QW gradually increases as the growth temperature of the sample decreases, as expected, although the indium fractions vary across the 5 QWs in each individual sample. The average indium fractions across all 5 QWs are 0.13 ± 0.01, 0.16 ± 0.01, and 0.24 ± 0.01 for the samples with the Low, Med, and High indium contents (Table I), respectively. The impact of APT laser energy on chemical compositions of group III-nitrides has been widely investigated, with studies addressing binary GaN[27] and ternary AlGaN[23] and InAlN.[37] The measurement of nitrogen content (i.e., stoichiometry) has been found to be dependent on the applied laser energies and thus the evaporation fields. However, no large variation of the measured indium to gallium ratio (In/Ga) in

TABLE I. Summary of measured indium contents (from APT), geometric parameters of QW structures (from STEM), and optical properties.

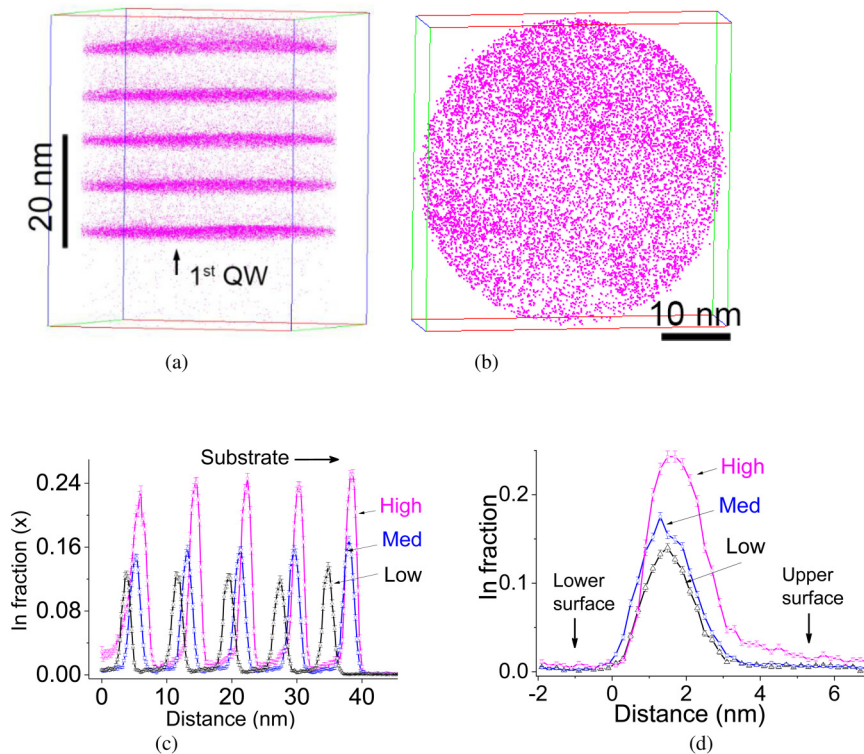|	APT		STEM		PL	
	In fraction	FD analysis	QW (nm)	Barrier (nm)	Peak (eV)	FWHM (meV)
Low	0.13 ± 0.01	Random	2.1 ± 0.2	5.7 ± 0.2	3.038	121
Med	0.16 ± 0.01	Some evidence of nonrandomness	2.3 ± 0.2	5.8 ± 0.2	2.928	133
High	0.24 ± 0.01	Nonrandom	2.6 ± 0.3	5.7 ± 0.4	2.610	157

FIG. 2. (a) A three-dimensional APT reconstruction showing the indium atoms in the sample with the High indium content, (b) the second QW isolated from the data set in (a), seen in plan view, (c) one-dimensional indium distribution profiles across 5QWs for all samples with different indium contents, and (d) the indium profiles across the second QW for all samples calculated using a proximity histogram approach based on the lower interface with an indium fraction threshold of 0.03 for Low indium content sample and 0.05 for the other two samples.

InGaN[21] was observed across a modest laser energy range.[37] In the present work, the influence of laser energy on the measured indium fractions cannot be excluded, but errors are expected to be negligible given the applied laser energies. In addition, the measured In/Ga fractions from APT are consistent with the XRD analysis, which gives values of 0.14 ± 0.03, 0.18 ± 0.03, and 0.28 ± 0.03 for the samples with Low, Med, and High indium contents, respectively. In Fig. 2(c), a noticeably reduced thickness across the 5 QWs is seen in the sample with the Low indium content, which is consistent with the STEM analysis in Fig. 1. Figure 2(d) represents comparisons of the second QWs across the three samples, in which the indium fraction through the QW thickness was calculated using a proximity histogram (proxigram) approach, which measures composition as a function of distance from a defined isoconcentration surface. This surface of reference was based on the lower InGaN/GaN interfaces defined by an indium fraction threshold of 0.03 for the Low indium content sample and 0.05 for the other two samples. In all three samples, the QWs have a relative abrupt lower interface and a less abrupt upper interface with some indium incorporation into the barrier. This is consistent with previous analysis on other crystal orientations.[22,38,39]

The statistical FD analysis of the indium distribution has been carried out on the first three QWs for each sample. The APT data were divided into sampling bins of size ranging from 25 to 200 atoms (In and Ga atoms only) with a step size of 25 atoms. The FD analysis of the Low indium content sample indicates that the p-values of all 24 analyzed cases are ubiquitously larger than 5%, providing no evidence for an indium distribution which deviates

from statistical randomness. However, in the High indium content sample, there are 20 cases out of total 24, where the p-values are less than 5%, providing ample evidence of a nonrandom indium distribution. The outcomes of the FD analysis are summarized in Table I. A less clear-cut situation has been found in analyzing the Med indium content sample, in which the p-value is dependent on each analyzed case, ending up 11 cases out of 24 with the p-value less than 5%. Figure 3 illustrates the FD analysis with the 75-atom bin size for the Low [(a) and (b)] and High [(c) and (d)] indium content samples. Figures 3(a) and 3(c) are the FD graphs, and Figs. 3(b) and 3(d) are the frequency difference between the measured and theoretical random distribution values. For the Low indium content sample, for which the χ^2 analysis reveals that indium atoms were statistically randomly dispersed, the frequency difference plot is noisy with no pronounced peaks or troughs above the noise. For the High indium content case, the frequency difference plot reveals excess volumes with indium content significantly above and below the mean, and a lack of material with the mean indium content, as is expected for a clustered sample, and consistent with the χ^2 analysis which indicated a statistically nonrandom indium distribution.

The modified NN analysis has the advantage of avoiding influence from through-thickness indium content variations, since the QW is projected into a single plane. Figure 4 depicts the indium atom distributions in the first QW in each of three samples. Figures 4(a) and 4(b) are color-coded two-dimensional indium atom maps, as-measured and after randomization, respectively, for the case of the High indium content sample. Compared to Fig. 4(a), a
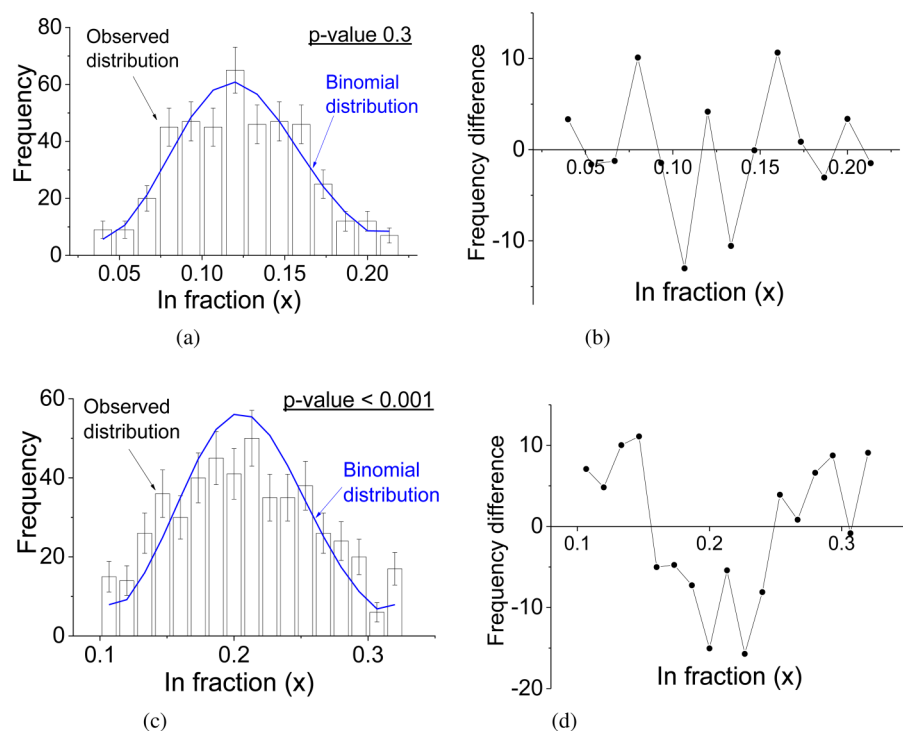
FIG. 3. Frequency distribution (FD) analysis (75 atom-block size) of the indium distribution in the second QW from (a) and (b) the Low indium content sample (p-value 0.3), and (c) and (d) the High indium content sample (p-value < 0.001). (a) and (c) are the frequency distributions as a function of indium fraction, whereas (c) and (d) are the distribution of frequency difference between measured distribution and the appropriate binomial distribution for a random alloy in each of the two samples.

more uniform indium distribution can be visually observed in the randomized maps in Fig. 4(b). Figures 4(c) to 4(e) are the kNN (k = 5, 10, 25, 50) analysis of the three samples. For the case of the Low indium content sample, the as-measured indium distributions match with their corresponding theoretical distributions well, with a negligible deviation [Fig. 4(c)]. However, a gradually increasing departure from the corresponding theoretical random distribution can be seen from the case of Med indium content to that of High indium content. This analysis aligns well with the FD analysis.

Overall, although it is difficult to say definitively whether the indium distribution in the Med sample deviates from randomness, the data from across the three samples indicate an increased tendency toward clustering as the indium content increases. In the Secs. III A 1 and III B, especially in the theoretical description of the optical properties, we direct our attention to the impact of clustering on the electronic and optical properties of m-plane InGaN QWs with increasing indium content. The influence of purely random alloy fluctuations has been discussed in detail in Refs. 42 and 46. We review and compare our previous results (random alloy) on the Med indium content sample to the findings observed here (indium clustering) in Sec. III B and discuss how an improved theory–experiment comparison might be expected when including both random alloy fluctuations and indium clustering in the theoretical description.

2. Experimentally determined optical properties

As stated previously, the low temperature optical properties of the structures that we have characterized by APT have been reported in detail in our previous publication.[20] In this previous study, we concentrated on the differences between a series of InGaN QWs grown either on a-plane or m-plane free standing bulk GaN substrates. In this paper, we are concerned with the m-plane structures and focus on how indium clustering and temperature affect the optical properties, especially the DOLP of these structures. We are interested in trends in the optical properties with increasing indium content. Thus, we focus here, in contrast to our previous work,[20] on three m-plane samples, which have been denoted here by Low, Med, and High indium content since they allow us to cover a representative indium content range usually found in InGaN/GaN QWs. These samples correspond to the samples denoted M1, M2, and M4 in Ref. 21. The relevant m-plane samples denoted as Low, Med, and High indium content systems reveal emission peak PL energies at T = 10 K of 3.038 eV, 2.928 eV, and 2.610 eV, respectively. Of particular note is the large spectral width of the emission with values of the full width at half maximum height (FWHM) of 121 meV, 133 meV, and 157 meV for the Low, Med, and High indium content samples, respectively, as shown in Table I. In time-resolved PL, all these systems exhibit single exponential decays with time constants of ∼300 ps which are unchanged across the individual spectra. Also at the temperature of T = 10 K, all the samples exhibited a high DOLP across the spectra in excess of 0.9. We will discuss the low temperature results along with results from measurements at elevated temperatures in more detail below. Overall, it is worth noting here that in our previous work, similar a-plane samples showed lower DOLPs than their m-plane counterparts.
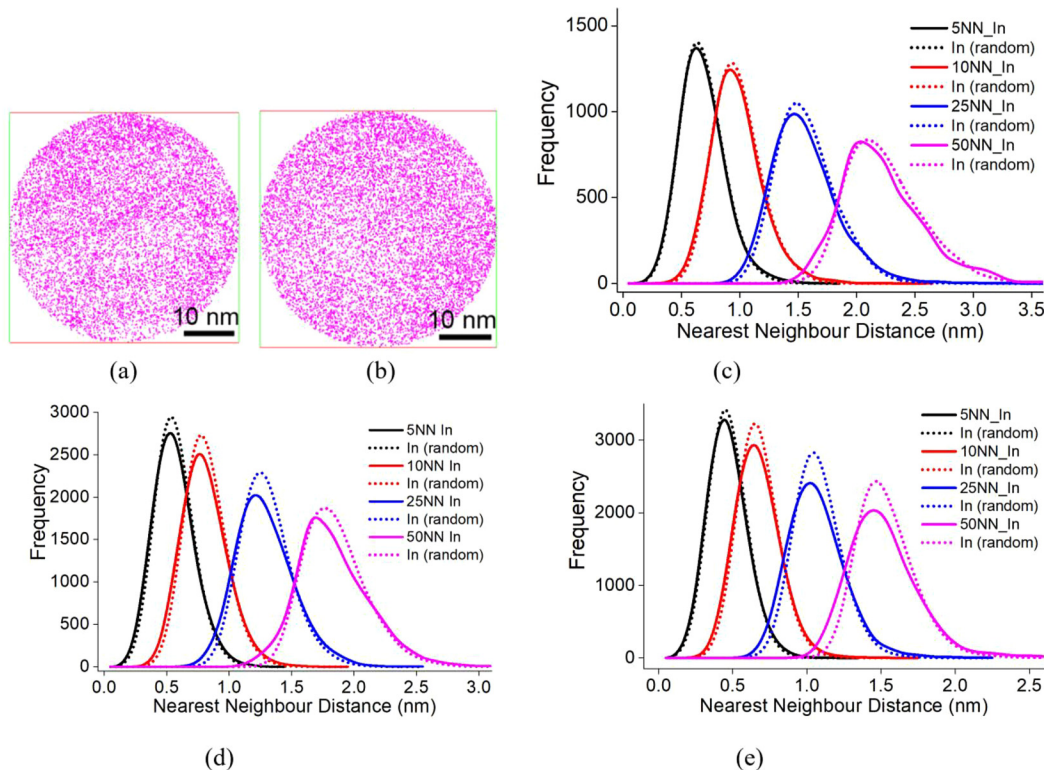
FIG. 4. Modified nearest neighbor (NN) distribution analysis of the first QW in each of the three samples. (a) and (b) show the two-dimensional In distribution of the first QW of the sample with the High indium content, (a) as-measured and (b) after randomization, respectively. (c)–(e) show the kNN analysis of the Low, Med, and High indium content samples, respectively, for k = 5, 10, 25, and 50. Comparison of the solid lines (measured distribution) with the dotted lines (random distribution) shows that the measured indium distribution increasingly deviates from that for a random alloy as the indium content increases.

We also report on the temperature dependence of the emission polarized perpendicular and parallel to the c-axis which allowed us to determine the DOLP $\rho(T)$, Eq. (1), at elevated temperatures. In Fig. 5, we present the temperature dependence of the spectra when detecting the $I_\perp$ and $I_\parallel$ components of the emission for the High indium content sample. Similar data for the other samples studied show qualitatively the same general temperature dependencies of the two different polarizations. It should be stressed that the spectra of the two components which are shown in Figs. 5(a) and 5(b) have radically different numerical ranges on the y axes so that for all the temperatures, the peak values of $I_\perp$ are greatly in excess of the peak values of $I_\parallel$. At 10 K, the value of DOLP $\rho(T = 10\,K)$, Eq. (1), at the peak of the $I_\perp$ spectrum is 0.98, and it should be noted that the peak emission for both polarizations of light is at the same energy of 2.602 eV. A similar observation has been made for the Low and Med indium content samples with similar DOLP values. We have already seen in our previous combined experimental and atomistic theoretical analysis that carrier localization in the hole ground states is sufficient to explain these high DOLP values at low temperatures.[42,46]

Turning now to experimental results at elevated temperatures, the situation is radically changed as revealed by the contrasting shifts of the peak energies of the spectra associated with the two polarizations of light. The peak energy of the much stronger $I_\perp$ emission shifts progressively to lower energy with increasing temperature. We assign this behavior to the combined effects of the temperature dependence of the InGaN bandgap and the thermally induced redistribution of the carriers among the distribution of localized states. However, the peak of the spectra of the $I_\parallel$ emission initially follows the temperature dependence of the $I_\perp$ light but then at higher temperatures the peak moves to higher energies. This behavior at the higher temperatures is caused by the thermal occupation of hole states that emit mainly $I_\parallel$ light. In a simplified valence band picture, this could be described as a population of the second valence subband which is dominated by $|Z\rangle$-like basis states (crystal field split-off band). We return to this classification below when discussing the theoretical DOLP results. Overall, our experimental studies show that the DOLP at the high temperatures is a complex function of the degree of inhomogeneous broadening of the spectra and the alloy disorder induced band mixing effects across a wide energy range in the "valence band." At the peak of the PL spectra, the values of the DOLP are 0.79, 0.92, and 0.88 as a function of increasing In fraction in the QWs.
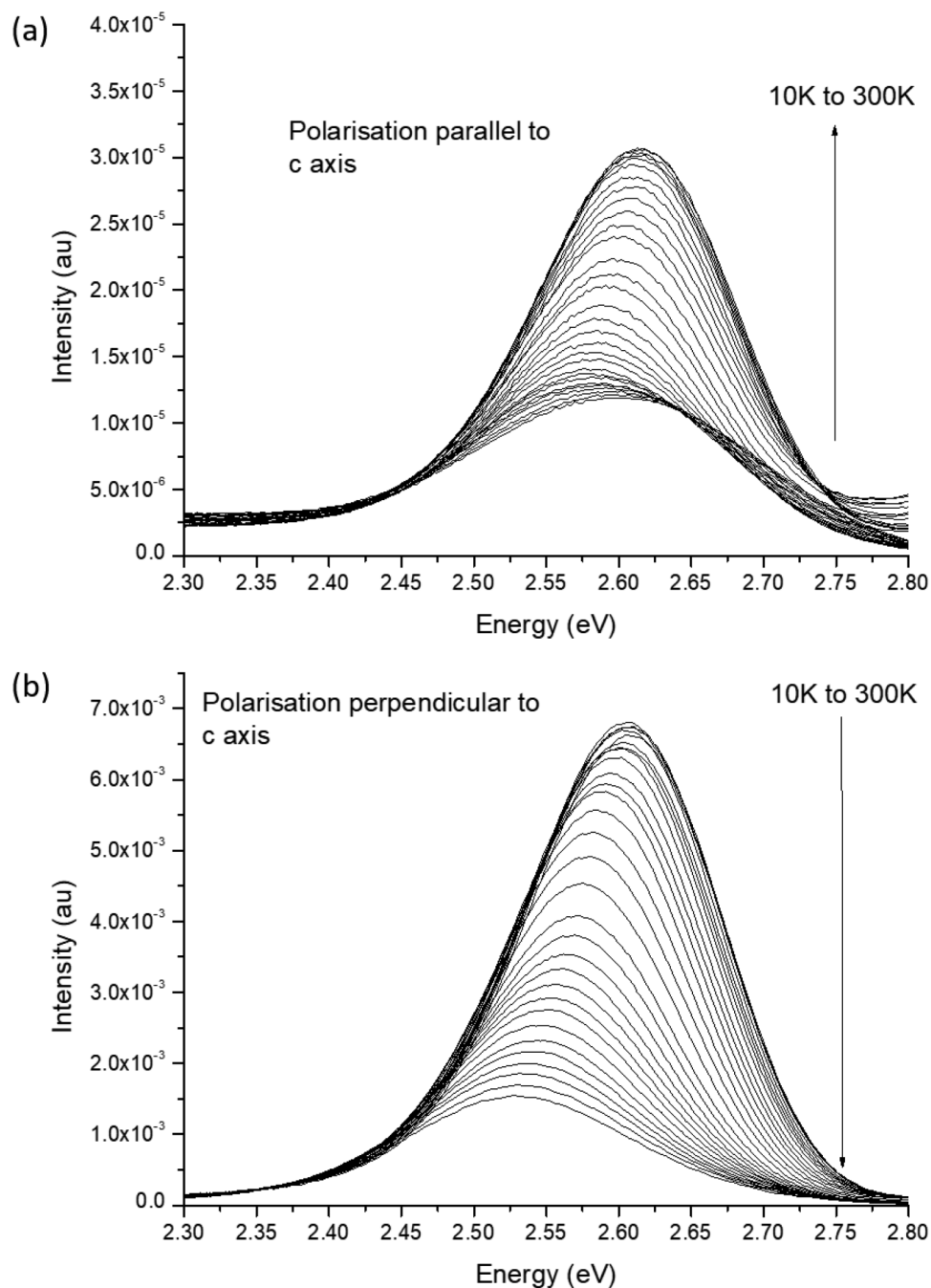
FIG. 5. Variation in the emission spectrum of the High indium content sample with temperature for emission polarized (a) parallel to the c-axis and (b) perpendicular to the c-axis.

B. Theoretical calculations

From the APT data presented in Sec. III A, it can be concluded that the nonpolar InGaN/GaN QW systems studied, at least for higher indium contents, exhibit indium clustering effects. Since indium-rich regions can lead to carrier localization, our theoretical modeling now targets the question of how these clusters impact the electronic and optical properties of the QWs studied here. As already briefly discussed in Sec. II (B), in order to address the observed indium-rich regions, a 3D $\mathbf{k} \cdot \mathbf{p}$ model is applied. It is now necessary to extract the parameters of a typical indium-rich region from the APT data to provide input into the calculations. To achieve this, the indium contents associated with regions with

composition in excess of that which would be expected from a binomial distribution were found based on the composition ranges with significant positive deviations in frequency difference plots such as that in Fig. 3(d). Isoconcentration surface plots of individual QWs were then generated for several compositions in this range. For example, for the High indium content sample whose data are shown in Fig. 3(d), the frequency difference is positive for indium fractions from 0.25 upward. For this sample, isoconcentration surface plots were generated at In compositions of 0.26, 0.28, 0.31, and 0.35 with a voxel size of 0.5 nm and a delocalization of 2.0 nm. Such plots suggested that there are regions present in the High indium content QWs with locally increased indium content which have diameters between one and a few nanometers and composition grading from a value approaching the average composition of the QW to a value of 0.35 or more. A typical set of isosurface plots for one of these high indium content regions is shown in Fig. 6. Although we acknowledge that the specific parameters used in generating the isoconcentration surface will inevitably influence the details of the observed region to some extent, we have used data like that presented in Fig. 6 and various other similar locations to create a simple model which treats the indium-rich regions in
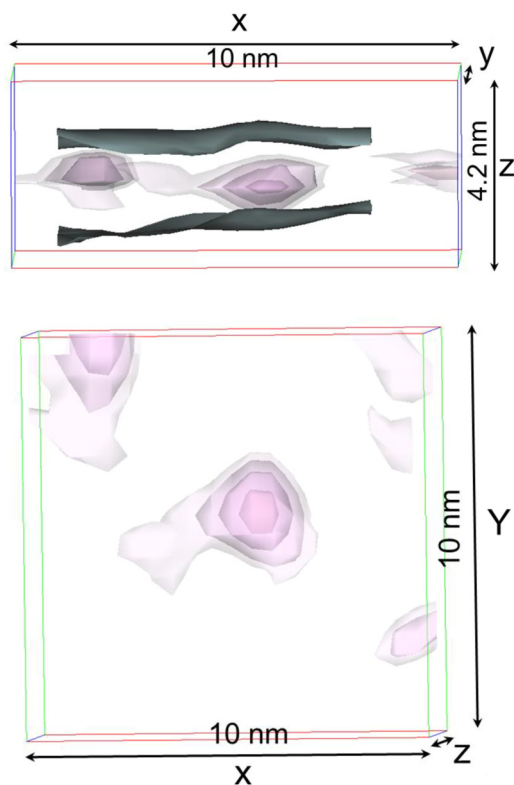

FIG. 6. A typical high indium content region in the sample with the highest indium content delineated by isoconcentration surfaces. From innermost to outermost the isosurfaces are set at compositions of x = 0.35; 0.31; 0.28; 0.26. The voxel size is 0.5 nm, and the delocalization is 2.0 nm.

the High indium content sample as ellipsoids, the details of which will be discussed below. For the Med indium content sample, indium-rich regions with a similar form, and with a maximum indium content of around 0.28, have been identified in the APT data, in the parts of the data set where the χ^2 analysis indicated the presence of a nonrandom indium distribution, and a similar model is thus applied.

Hence, building on the APT data, within our 3D $\mathbf{k} \cdot \mathbf{p}$ approach, the indium-rich regions inside the InGaN wells are treated as quantum dot (QD) like structures. Thus, the system is approximated by a dot-in-a-well (DWELL) structure. More specifically and consistent with the experiment, the indium-rich regions have been modeled as ellipsoidal QDs embedded in the QW. Here, we have performed calculations for both the Med and the High indium content systems. In the High indium content sample, and following the experimental data, the indium metallic fraction content inside the dot gradually changes from x = 0.35 at the dot center to 0.25 at the dot boundary/QW region. The indium content in the surrounding well is kept constant at 0.25. For the Med indium content sample, the same approach has been used, but the indium content inside the dot region changes from x = 0.16 at the dot/QW boundary to 0.28 in the dot center. The indium content of the surrounding well is kept constant at 0.16. For both systems, a linear variation of the indium content between the dot center and well region is applied. This composition profile is now applied to dots with different in-plane dimensions, which allows us to study the impact of the cluster/dot size on the results. For both the Med and High indium content structures, the width of the QW and the height of the ellipsoid are kept constant at 2.6 nm and 2.0 nm, respectively. Initially, the major and minor axes of the ellipsoidal inclusion inside the well have been assumed to be identical (circular in-plane shape). In general, the dot size is defined as the distance between points along the major, minor (both in-plane), and the growth direction (height) where the indium content reaches the indium content values of the surrounding well. A schematic illustration of the DWELL system is given in Fig. 7. Since it is unlikely that all (or even the majority) of the clusters/dots will exhibit in-plane circular symmetry, the impact of changes in the in-plane geometry on, for instance, the DOLP have also been studied. Therefore, the major and minor axes of the ellipsoidal dot have been varied between 6.0 and 3.0 nm. More details are given below when the calculated DOLP values are compared to experimental data. In general, the simulations have been carried out on a supercell with periodic boundary conditions; the dimension of the supercell is $25 \times 25 \times 15$ nm^3. The grid has been discretized in the growth plane with a step size of 0.2 nm; along the growth direction the step size is 0.1 nm.

Having discussed how the APT structural data have been incorporated in the 3D $\mathbf{k} \cdot \mathbf{p}$ analysis, in a first step, we study the impact of the indium-rich regions on the electronic structure in terms of carrier localization effects. Figure 8 displays isosurfaces of the electron (blue) and hole (green) ground state charge densities for the Med [Fig. 8(a)] and High [Fig. 8(b)] indium content system, respectively. The isosurfaces correspond to 25% of the maximum values. As a guide to the eye, the dashed lines indicate the different interfaces (dot-well and well-barrier). For these calculations, the major and minor axes of the ellipsoid are equal to 6 nm
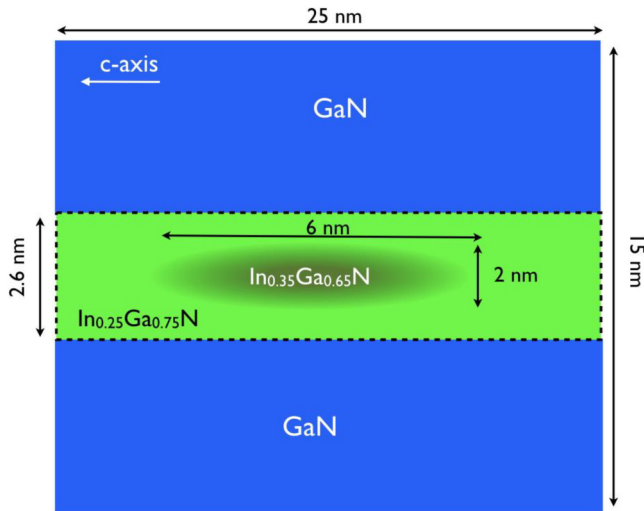
FIG. 7. Schematic illustration of the dot-in-a-well system underlying the theoretical calculations. High indium content system has been used as an example.

(in-plane circular symmetric dot). From Fig. 8, we conclude that the indium-rich regions act as carrier localization centers, for both electrons and holes. This effect is also present when the size of the dot in the growth plane is reduced to 3 nm (not shown). Consequently, even without an atomistic description of the underlying InGaN alloy, our calculations reveal that electron and hole wave functions are localized in the same spatial position facilitated by the indium-rich regions. Given the presence of indium-rich regions in the well, in an atomistic picture, the likelihood of
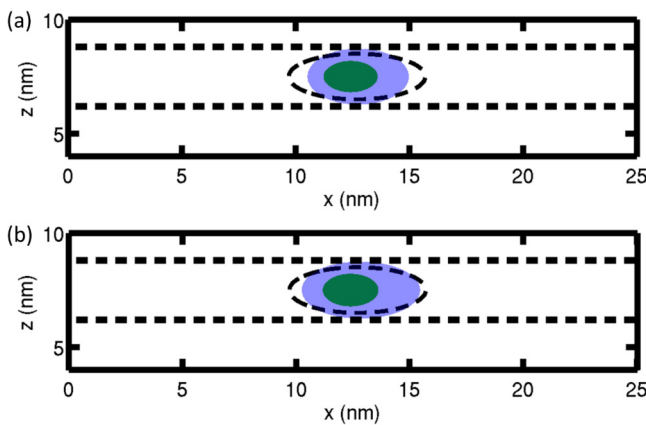

FIG. 8. Isosurfaces of the electron (blue) and hole (green) ground state charge densities. Note, charge densities are basically located in the same spatial position, thus the blue and green isosurfaces are overlapping. The charge densities are plotted at 25% of their respective maximum values. The dashed-lines indicate the QW barrier interfaces as well as dot-well interfaces. Results are here shown for (a) the Med indium content system and (b) the High indium content system.

In-N-In chains is increased. Atomistic calculations have already shown that these chains lead to strong hole wave function localization effects.[40,41] Therefore, our 3D $\mathbf{k} \cdot \mathbf{p}$ result shows that electrons and holes are localized in the same spatial region due to the presence of indium-rich regions, which is expected to remain unchanged even if the microscopic features of the alloy were be included in our calculations.

Another important consequence of the above finding is that this behavior supports exciton localization effects. Such a situation has been observed in atomistic calculations[42] and is consistent with experimental observations, e.g., single exponential decay transitions in time-resolved PL studies. Even though our 3D $\mathbf{k} \cdot \mathbf{p}$ calculations do not account for excitonic effects, the fact that electrons and holes are localized in the same spatial position will not be changed if Coulomb effects are included in the description. Furthermore, given that electron and hole localization effects will only be slightly affected by changes in the indium cluster size, especially when considering the attractive Coulomb interaction, fast radiative lifetimes are expected, consistent with our earlier experimental observations.[20]

In a second step, the theoretical framework has been used to study the DOLP of the nonpolar InGaN/GaN QW systems with Med and High indium contents. To gain insight into this question and also into the temperature dependence of the DOLP, we follow Refs. 43 and 44 and utilize here the spontaneous emission rates for different light polarization vectors $\mathbf{a}$ and temperatures T. In general, the spontaneous emission rate R_{sp} is defined in Ref 45 as

$$R_{sp} = \int d(\hbar\omega) \frac{2e^2 n\hbar\omega}{m_0^2 \varepsilon_0 c^3 \hbar^2} \sum_{i,j} |\mathbf{a} \cdot \mathbf{p}_{i,j}|^2$$
$$\times \frac{1}{\sqrt{2\pi}\sigma} \exp\left[\frac{-(\Delta E_{i,j} - \hbar\omega)^2}{2\sigma^2}\right] f^e(E_i^e) f^h(E_j^h). \quad (2)$$

Here, e, m_0, ε_0, c, n, and $\hbar$ denote electron charge, free electron mass, vacuum permittivity, vacuum speed of light, refractive index, and reduced Planck's constant, respectively. The transition energies are given by $\Delta E_{i,j}$, which is the energetic separation between the electron state i and the hole state j. The inhomogeneous broadening parameter is denoted by σ and is assumed to be 100 meV for this study, which gives a good description of the typical magnitude of the experimentally measured FWHM in this work for m-plane InGaN/GaN QWs. The momentum matrix element between electron state i and hole state j is given by $|\mathbf{a} \cdot \mathbf{p}_{i,j}|^2$, which also contains the light polarization vector $\mathbf{a}$. With increasing temperature T, excited electron and hole states are populated and this effect has been accounted for by Fermi-functions for electrons and holes, which are denoted by f^e and f^h, respectively.[44] Since indium-rich clustered regions have been modeled as QD-like structures, a QD-like description of the spontaneous emission rate has been used in the calculations.

Equipped with this knowledge about the temperature dependence of spontaneous emission rate, the DOLP can now be obtained through Eq. (1), where set $I_\perp(T) = R_{SP}^\perp(T)$ and $I_\parallel(T) = R_{SP}^\parallel(T)$. Here, $R_{SP}^\parallel(T)$ ($R_{SP}^\perp(T)$) denote the temperature dependent emission rate for a light polarization vector parallel (perpendicular) to the

wurtzite c-axis. Using this approach, calculated and measured DOLP can be compared for different temperatures T.

We start here with the discussion of low temperature ($T = 10$ K) theoretical results. When modeling both the Med and the High indium content samples, incorporating the DWELL structures and assuming circular in-plane geometry of the dot, we find that the emitted light, in line with the experiment, is predominantly polarized in the plane perpendicular to the c-axis. The corresponding DOLP values ρ are 0.98 (98%) and 0.99 (99%) for the Med and High indium content samples, respectively. These high DOLP values reflect the orbital character of mainly the hole ground states. For instance, the hole ground state, depicted in Fig. 8(a) (Med indium content system), exhibits an orbital character decomposition of $|X\rangle = 0.016$ (1.6%), $|Y\rangle = 0.954$ (95.4%), and $|Z\rangle = 0.030$ (3%). For the hole ground state in the High indium content regime, depicted in Fig. 8(b), the orbital character reads $|X\rangle = 0.010$ (1.0%), $|Y\rangle = 0.960$ (96%), and $|Z\rangle = 0.030$ (3.0%). To study the impact of dot shape anisotropies on the DOLP, the in-plane symmetry of the ellipsoidal, indium-rich region has been modified. To this end, the cluster is squeezed along the two in-plane directions. More specifically, the major and minor axes vary between 3 and 6 nm. The major axis of the ellipsoid is always aligned to the wurtzite c-axis. Overall, our calculations reveal that the DOLP is unaffected by these shape anisotropies, indicating that the exact dimensions of the fluctuations are of secondary importance, at least for the DOLP of these systems at low temperature. Therefore, our theoretical observations here are consistent with the experimental finding of very high DOLP values at these temperatures.

This analysis also sheds light on further aspects of the experimental data. While the DOLP stays approximately constant when changing the volume of the dot, the transition energies are significantly affected. When reducing the in-plane dimensions of the model dot/cluster, we find variations in the transition energies with respect to the symmetric dot of 40–60 meV. Statistical variations in the indium cluster size and shape will thus lead to significant variations in the transition energies and consequently to a broadening of the PL linewidth. Atomistic investigations, neglecting clustering effects in an InGaN/GaN m-plane system with x = 0.17 indium, resulted in a FWHM maximum value of approximately 100 meV.[42,46] These theoretical studies only accounted for random alloy fluctuations. For the Med indium content sample studied here, with a measured indium content of $\sim$x = 0.16 from APT or $\sim$x = 0.18 from XRD, the experimentally observed FWHM is larger than the calculated value, at 133 meV. Thus, taking all these aspects together, we expect that variations in the electron and hole energies are increased by the combined effect of random alloy fluctuations and the presence of indium clusters with statistical variations in cluster shape, size, and indium content. This, in turn, will lead to an increase of the theoretically predicted FWHM value in Refs. 42 and 46, where clustering effects are neglected, thus improving the agreement between experiment and theory. Overall, this investigation reveals that for a detailed understanding of the electronic and optical properties of m-plane InGaN/GaN QW systems, clustering effects become increasingly important with increasing indium contents.

Having discussed low temperature data, we focus our attention now on DOLP values at elevated temperatures. The experimental data presented above reveals also high DOLP values at elevated

temperatures using the PL peak values of $I_{\parallel}$ and $I_{\perp}$. To shed light on this question, the spontaneous emission $R_{sp}(T)$ has been used to calculate the DOLP as a function of temperature T for the Med and High indium content systems. For this study, the in-plane cluster diameter has been kept constant at 6.0 nm in both in-plane directions. The calculated DOLP values, ρ, are displayed in Fig. 9 as a function of the temperature T. The (red) circles denote the data for the High indium content system, while the (blue) triangles show the results for the Med indium content system. Several aspects of this data are now of interest. First, up to $T = 75$ K, the DOLP stays approximately constant in both systems. We attribute this to the fact that only hole states of the same orbital character are being significantly populated. For temperature values above $T = 75$ K, carriers start to populate states where band mixing effects become more important. This results in a decrease in the DOLP. Usually, this can be attributed to states which have a higher contribution of the crystal field split off band, which is dominated by $|Z\rangle$-like orbitals oriented along the wurtzite c-axis. Looking at Eq. (2), the increase in temperature leads to the situation that states which are predominantly $|Z\rangle$-like in character are being populated. This results in a decrease in the spontaneous emission rate $R_{SP}^{\perp}(T)$, while the rate $R_{SP}^{\parallel}(T)$ starts to increase. Consequently, the DOLP decreases with increasing temperature. The observation that the decrease in DOLP happens at a slower rate for the High indium content system, when compared to the Med indium content structure system, in part, from the effect that with increasing indium content the anisotropic strain in the growth plane increases. In addition to this effect, enhanced confinement effects in the higher indium content system give rise to an increase in the energetic separation of $|X\rangle$-, $|Y\rangle$-, and $|Z\rangle$-like states due to the differences in their effective masses. Since the orbital character of the different states and their energetic separation is key for the temperature dependence of the DOLP, the DOLP in the High indium content sample is expected to stay constant over a wider temperature range when compared to the Med indium content system. Based on all
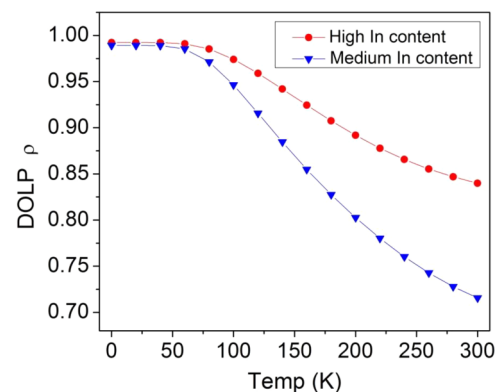
FIG. 9. Calculated degree of optical linear polarization as a function of the temperature (Temp) T in Kelvin. The (red) circles give the results for the High indium content system, while the (blue) triangles give the results for the Med indium content system.

this, higher DOLP values at room temperature are expected for the High indium content system again compared to the Med indium content structure. At $T = 300$ K, the calculated DOLP value is 0.71 (71%) and 0.84 (84%) for the Med and High indium content system, respectively. For the High indium content system, the theoretical value is in good agreement with experimental data of 0.88 (88%) on this sample. However, the calculated value for the Med indium system is noticeably smaller than the peak DOLP value extracted in the experiment of 0.92 (92%) at 300 K. We attribute this observation to the following factors. First, it should be noted that in contrast to the High indium content system, the Med indium content system, in terms of the indium atom distribution, is borderline between a random and clustered system. In the theoretical modeling, our 3D continuum-based approach accounts for the effects of the clusters but neglects random alloy effects. Therefore, carrier localization effects due to random alloy fluctuations are not accounted for here. As we have shown before, using atomistic tight-binding calculations, carrier localization effects due to random alloy fluctuations can lead to a high DOLP value over an energy range much wider than the typical valence subband splitting expected in a standard 1D continuum-based description of an InGaN QW system.[44] A similar effect will contribute to the temperature dependence of the DOLP. Based on all these arguments, we expect that the presented theoretical results reflect a lower bound for the DOLP at 300 K. Overall, it is important to note that our analysis shows that indium clustering effects still support high DOLP values. This is a crucial conclusion, since experimentally a-plane InGaN/GaN QWs, which exhibit a similar level of clustering, have vastly different optical characteristics than their m-plane counterparts. For instance, the DOLP measured in a-plane InGaN/GaN QWs is in general much lower. Our investigation thus indicates that indium-rich regions are unlikely to be the cause of the low DOLP values in a-plane systems, otherwise similar effects should also be observed in the m-plane structures studied here.

IV. CONCLUSION

In m-plane InGaN QWs grown on bulk m-plane GaN substrates, a random indium distribution is present for indium contents of x = 0.14 and below. However, as the indium content is increased there is an increasing tendency for the indium distribution to deviate from randomness with the formation of nanometre scale indium clusters. The results of our 3D $\mathbf{k} \cdot \mathbf{p}$ simulations indicate that the electron and hole will be colocalized within the indium clusters, leading to short radiative recombination lifetimes, as has previously been observed experimentally.[20] The presence of indium clusters and statistical variations in their shape, size, and indium content help one to explain the very large emission linewidths which are seen in these samples. According to our earlier atomistic calculations, these values exceed those which would be expected from a structure where the indium atoms are randomly distributed. Also, our calculations here reveal very high DOLP values in nonpolar QWs, even when taking indium clustering effects into account. This is consistent with the experimental observations of high DOLP values from the m-plane samples studied here, irrespective of indium content, but inconsistent with our earlier suggestion that the presence of clusters

in nonpolar a-plane QWs might lead to the lower DOLPs observed in that system. The question of why the a-plane material exhibits a lower DOLP than the m-plane material hence remains unresolved. Overall, however, we note that the presence of clustering can have a significant effect on the optical properties of nonpolar QWs and that APT is increasingly established as an important tool to investigate this phenomenon.

REFERENCES

[1] M. Auf der Maur, A. Pecchia, G. Penazzi, W. Rodrigues, and A. Di Carlo, Phys. Rev. Lett. **116**, 027401 (2016).
[2] C. Humphreys et al., Ultramicroscopy **176**, 93 (2017).
[3] S. F. Chichibu et al., Nat. Mater. **5**, 810 (2006).
[4] T. Sugahara et al., Jpn. J. Appl. Phys. **37**, L398 (1998).
[5] D. Graham, A. Soltani-Vala, P. Dawson, M. Godfrey, T. Smeeton, J. Barnard, M. Kappers, C. Humphreys, and E. Thrush, J. Appl. Phys. **97**, 103508 (2005).
[6] S. Hammersley, D. Watson-Parris, P. Dawson, M. Godfrey, T. Badcock, M. Kappers, C. McAleese, R. Oliver, and C. Humphreys, J. Appl. Phys. **111**, 083512 (2012).
[7] Y.-H. Cho, G. Gainer, A. Fischer, J. Song, S. Keller, U. Mishra, and S. DenBaars, Appl. Phys. Lett. **73**, 1370 (1998).
[8] W. E. Blenkhorn, S. Schulz, D. S. P. Tanner, R. A. Oliver, M. J. Kappers, C. J. Humphreys, and P. Dawson, J. Phys. Condens. Matter **30**, 175303 (2018).
[9] Y. Narukawa, Y. Kawakami, M. Funato, S. Fujita, S. Fujita, and S. Nakamura, Appl. Phys. Lett. **70**, 981 (1997).
[10] M. J. Galtrey, R. A. Oliver, M. J. Kappers, C. J. Humphreys, D. J. Stokes, P. H. Clifton, and A. Cerezo, Appl. Phys. Lett. **90**, 061903 (2007).
[11] K. H. Baloch, A. C. Johnston-Peck, K. Kisslinger, E. A. Stach, and S. Gradečak, Appl. Phys. Lett. **102**, 191910 (2013).
[12] F. Bernardini, V. Fiorentini, and D. Vanderbilt, Phys. Rev. B **56**, R10024 (1997).
[13] S. Nakamura, Science **281**, 956 (1998).
[14] O. Ambacher et al., J. Phys. Condens. Matter **14**, 3399 (2002).
[15] S. K. Patra and S. Schulz, Phys. Rev. B **96**, 155307 (2017).
[16] M. Leroux, N. Grandjean, M. Laügt, J. Massies, B. Gil, P. Lefebvre, and P. Bigenwald, Phys. Rev. B **58**, R13371 (1998).
[17] T. Takeuchi et al., Appl. Phys. Lett. **73**, 1691 (1998).
[18] S. P. DenBaars et al., Acta Mater. **61**, 945 (2013).
[19] K. A. Bulashevich, A. V. Kulik, and S. Y. Karpov, Phys. Status Solidi A **212**, 914 (2015).
[20] D. Kundys, D. Sutherland, M. J. Davies, F. Oehler, J. Griffiths, P. Dawson, M. J. Kappers, C. J. Humphreys, S. Schulz, F. Tang, and R. A. Oliver, Sci. Technol. Adv. Mater. **17**, 736–743 (2016).
[21] S. Schulz T. Badcock et al., Phys. Rev. B **82**, 125318 (2010).
[22] F. Tang et al., Appl. Phys. Lett. **106**, 072104 (2015).
[23] T. Walther, X. Wang, V. C. Angadi, P. Ruterana, P. Longo, and T. Aoki, J. Mater. Res. **32**, 983 (2017).
[24] L. Rigutti, B. Bonef, J. Speck, F. Tang, and R. A. Oliver, Scr. Mater. **148**, 75–81 (2018).
[25] B. Bonef, R. Cramer, and J. S. Speck, J. Appl. Phys. **121**, 225701 (2017).
[26] F. Tang, J. S. Barnard, T. Zhu, F. Oehler, M. J. Kappers, and R. A. Oliver, Appl. Phys. Lett. **107**, 082104 (2015).
[27] R. A. Oliver et al., Appl. Phys. Lett. **103**, 141114 (2013).

[28]F. Tang, M. P. Moody, T. L. Martin, P. A. Bagot, M. J. Kappers, and R. A. Oliver, Microsc. Microanal. **21**, 544 (2015).

[29]S. K. Patra, O. Marquardt, and S. Schulz, Opt. Quantum Electron. **48**, 151 (2016).

[30]O. Marquardt, S. Boeck, C. Freysoldt, T. Hickel, S. Schulz, J. Neugebauer, and E. P. O'Reilly, Comput. Mater. Sci. **95**, 280 (2014).

[31]S. Schulz and O. Marquardt, Phys. Rev. Appl. **3**, 064020 (2015).

[32]S. K. Patra and S. Schulz, J. Phys. D Appl. Phys. **50**, 025108 (2017).

[33]M. A. Caro, S. Schulz, and E. P. O'Reilly, Phys. Rev. B **88**, 214103 (2013).

[34]M. Varela, A. R. Lupini, K. van Benthem, A. Y. Borisevich, M. F. Chisholm, N. Shibata, E. Abe, and S. J. Pennycook, Annu. Rev. Mater. Res. **35**, 539 (2005).

[35]P. Munroe, Mater. Charact. **60**, 2 (2009).

[36]T. Smeeton, M. J. Kappers, J. Barnard, M. Vickers, and C. J. Humphreys, Appl. Phys. Lett. **83**, 5419 (2003).

[37]L. Mancini, N. Amirifar, D. Shinde, I. Blum, M. Gilbert, A. Vella, F. Vurpillot, W. Lefebvre, R. Lardé, E. Talbot, P. Pareige, X. Portier, A. Ziani, C. Davesnne, C. Durand, J. Eymery, R. Butté, J.-F. Carlin, N. Grandjean, and L. Rigutti, J. Phys. Chem. C **118**, 24136 (2014).

[38]T. Prosa, P. Clifton, H. Zhong, A. Tyagi, R. Shivaraman, S. DenBaars, S. Nakamura, and J. Speck, Appl. Phys. Lett. **98**, 191903 (2011).

[39]M. J. Galtrey, R. A. Oliver, M. J. Kappers, C. J. Humphreys, P. H. Clifton, D. Larson, D. W. Saxey, and A. Cerezo, J. Appl. Phys. **104**, 013524 (2008).

[40]S. Schulz, O. Marquardt, C. Coughlan, M. A. Caro, O. Brandt, and E. P. O'Reilly, Proc. SPIE **9357**, 93570C (2015).

[41]P. R. C. Kent and A. Zunger, Appl. Phys. Lett. **79**, 1977 (2001).

[42]S. Schulz, D. P. Tanner, E. P. O'Reilly, M. A. Caro, T. L. Martin, P. A. J. Bagot, M. P. Moody, F. Tang, J. T. Griffiths, F. Oehler, M. J. Kappers, R. A. Oliver, C. J. Humphreys, D. Sutherland, M. J. Davies, and P. Dawson, Phys. Rev. B **92**, 235419 (2015).

[43]C. Mounir, U. T. Schwarz, I. L. Koslow, M. Kneissl, T. Wernicke, T. Schimpke, and M. Strassburg, Phys. Rev. B **93**, 235314 (2016).

[44]T. Wang, T. J. Puchtler, S. K. Patra, T. Zhu, J. C. Jarman, R. A. Oliver, S. Schulz, and R. A. Taylor, Sci. Rep. **7**, 12067 (2017).

[45]Y.-R. Wu, Y.-Y. Lin, H–H Huang, and J. Singh, J. Appl. Phys. **105**, 013117 (2009).

[46]S. Schulz et al., Appl. Phys. Lett. **109**, 223102 (2016).